Available online at www.sciencedirect.com
ScienceDirect
Nuclear Instruments and Methods in Physics Research B 251 (2006) 352–360
NIM B
Beam Interactions with Materials & Atoms
www.elsevier.com/locate/nimb

Measurements of the stopping forces for heavy ions in Ge, Ag and Au using novel 'polka-dot' detectors

T.D.M. Weijers-Dall [a,b,*], H. Timmers [c], K. Stenström [d], P. Persson [d], A. Pergjegjaj [d], X. Wang [d], M. Graczyk [e], T. Osipowicz [f], M.Q. Ren [f], D.J. O'Connor [a], H.J. Whitlow [d,g,h]

[a] School of Mathematical and Physical Sciences, The University of Newcastle, Callaghan NSW 2308, Australia
[b] Department of Electronic Materials Engineering, The Research School of Physical Sciences and Engineering, The Australian National University, Canberra ACT 0200, Australia
[c] School of Physical, Environmental and Mathematical Sciences, University of New South Wales at the Australian Defence Force Academy, Canberra ACT 2600, Australia
[d] Division of Nuclear Physics, Lund University, P. O. Box 118, SE-221 00 Lund, Sweden
[e] Division of Solid State Physics, Lund Institue of Technology, P. O. Box 118, SE-221 00 Lund, Sweden
[f] Centre for Ion Beam Applications, Department of Physics, National University of Singapore, 2 Science Drive 3, Singapore 117542, Singapore
[g] School of Technology and Society, Malmö Högskola, SE-205 06 Malmö, Sweden
[h] Department of Physics, University of Jyväskylä, P. O. Box 35 (YFL) FIN-40014, Finland

Received 3 November 2005; received in revised form 25 July 2006
Available online 7 September 2006

Abstract

Measurements of the stopping forces for ^{14}C, ^{14}N and ^{16}O ions in Ge and Au, for ^{14}N and ^{19}F ions in Ag, as well as for ^{19}F ions in Au have been made, respectively. A novel technique, reported recently, using PIN diodes coated directly with the stopping medium in a polka dot pattern was used. This provided a set of precise, self-consistent measurements on the same stopping medium. Results show small but significant deviations from SRIM stopping predictions and are also compared to a recently-developed empirical stopping force predictor.

PACS: 34.50.Bw

Keywords: Energy loss; Stopping force; Stopping power

1. Introduction

Fields such as ion beam analysis, ion beam modification of materials, and radiation therapy rely on the accurate prediction of the stopping forces in their targets. Theoretical prediction of stopping forces, particularly around the Bragg peak, is difficult due to the complexity of the processes involved [1]. Many of the best accepted predictors therefore employ semi-empirical methods that interpolate from experimental data [2–6]. In this context, the availability of accurate measurements of the stopping forces in technologically relevant targets for a range of projectile species and energies is crucial. For heavy ions, however, large discrepancies between independent stopping measurements are often observed and in many cases measurements have simply not yet been performed.

A novel method for the measurement of stopping forces has recently been developed, which employs PIN photodiodes that are coated directly with the stopping medium in a regular polka dot pattern [7]. This new method addresses some of the issues that currently limit the accuracy of stopping force measurements. One key problem that is

* Corresponding author. Address: Department of Electronic Materials Engineering, The Research School of Physical Sciences and Engineering, The Australian National University, Canberra ACT 0200, Australia. Tel.: +61 2 6125 4060; fax: +61 2 6125 0511.
E-mail address: tessica.dall@anu.edu.au (T.D.M. Weijers-Dall).

0168-583X/$ - see front matter © 2006 Elsevier B.V. All rights reserved.
doi:10.1016/j.nimb.2006.07.019

overcome is that for low-energy ion stopping measurements the stopping medium must be very thin, making impractical the use of self-supporting stopping media. With direct coating the stopping medium can be supported by the detector itself, with the added improvement in the control of the thickness and uniformity of the layer. Furthermore, the use of a regular polka dot pattern so that islands of the stopping medium are present on detector enables the simultaneous detection of ions that have passed through the stopping medium and lost energy and those that passed directly into the detector. The implicit relationship between the energy loss and reference measurements that results ensures experimental consistency.

The aim of this work is to use this new method to obtain a set of self-consistent stopping force measurements for low-energy heavy ions stopped in a selected number of technologically-relevant target materials.

2. Experimental details

Hamamatsu Si PIN photodiodes (model S-1223-01) have been employed throughout this work. In each case the cap has been removed and the detector coated directly with a patterned layer of the stopping medium. The coating method has been described previously [7]. Briefly, the detectors were coated by evaporating the element of interest through a 0.3 mm-thick stainless steel mask. The mask pattern has 500 μm diameter circular holes that were produced by laser cutting. To prevent damage to the active layer of the detector and the contact wire, the mask was positioned approximately 1 mm above the detector surface during the evaporation. Using this method, the quality of the polka dot layer is high [7]. Detectors coated with Ge, Au and Ag have been employed in this study, respectively. The thickness of the coating is different in each case (and has been determined), but is of the order of 250–300 nm.

Energy loss measurements have been performed for ^{14}C, ^{14}N, ^{16}O and ^{19}F ions. The measurements for ^{16}O ions were performed using the 14 MV tandem Pelletron accelerator at The Australian National University, while the remainder were carried out using the 3 MV tandem Pelletron accelerator at Lund University, Sweden. In both cases the experimental setup was such that the ion beam from the accelerator was directly incident on the detector. In doing so, the current from the accelerator must be reduced to between 10 and 100 ions per second. For the case of the Lund accelerator standard AMS techniques were employed to achieve this low current [7], while at the ANU accelerator an earlier established technique for beam current reduction employing defocussing and aperturing was employed [9]. Each method is described in detail in the cited reference and has been shown to successfully produce a stable, controllable, low current beam of monoenergetic ions.

The detector stage was the same in each case (transported between the labs). A pair of coated PIN diodes were mounted side by side facing the incident beam at the end of the beam line, with the diodes held in place using a pair of Teflon disks. A copper plate with two appropriately positioned 2 mm diameter apertures was situated 5 mm in front of the detectors and electrically grounded. The diodes were reverse-biased with an external voltage between 8 and 25 V. The voltage was chosen to result in minimal detector noise levels and maximum detector resolution. The detector signals were pre-amplified and then pulse shaped using a linear spectroscopy amplifier. The signals were subsequently digitized using an ADC and recorded using an MCA.

A multi-line alpha particle source was used to provide a thickness measurement for each of the coated detectors, as well as provide an energy calibration for the Lund measurements. For the ANU measurements the energy of the ions could be determined from the 90° analyzing magnet setting (uncertainty <0.1%). Three different alpha particle sources were available and employed for this purpose, respectively: a ^{228}Th source, an ^{241}Am source and a ^{226}Ra source. The relevant alpha source was mounted on an

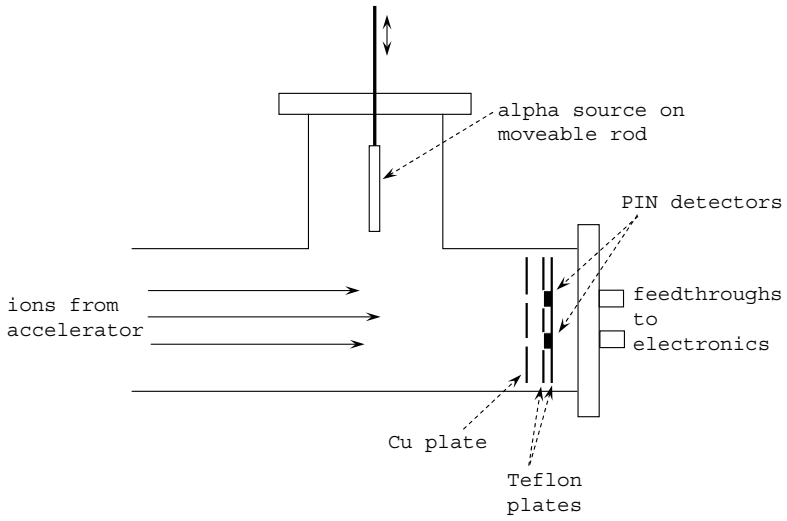

Fig. 1. Schematic view of detector stage viewed from above (not to scale).

Table 1
Summary of each of the measurements performed with the three coated detectors, respectively

Stopping medium	Ion species	Energy range (MeV)	Accelerator	Stripper	Detector bias (Volts)
Au	^{14}C[a]	6.3–10.2	Lund	Gas	8
	^{14}N[a]	6.2–7.8	Lund	Gas	8
	^{14}N	8.0–16.5	Lund	Gas	25
	^{16}O	19.4–49.5	ANU	Foil	20
	^{19}F	10.5–13.0	Lund	Foil	25
	^{19}F	2.3–11.8	Lund	Foil	25
Ge	^{14}C	6.2–10.1	Lund	Gas	8
	^{14}N	6.1–7.7	Lund	Gas	8
	^{16}O	20.2–49.8	ANU	Foil	20
Ag	^{14}N	3.8–9.2	Lund	Foil	25
	^{14}N	5.8–11.2	Lund	Foil	25
	^{19}F	5.4–10.8	Lund	Foil	25
	^{19}F	1.8–14.0	Lund	Foil	25

Details provided include the ion species and energy ranges measured, which accelerator was used, the stripping method employed, and the magnitude of the bias applied to the detector during the measurement.
[a] See note in text.

insertion rod (operated from outside the vacuum) so that the source could be moved in front of the detectors when required. This setup is illustrated in Fig. 1.

After the stopping measurements were completed the thickness of the polka dot layer on the detectors was mapped via Rutherford Backscattering, using a 2 MeV proton microbeam at the Centre for Ion Beam Applications at the National University of Singapore. This measurement was performed last of all because the damage introduced into the detector by the proton beam destroys the resolving power of the detector.

For clarity, Table 1 provides a summary of the relevant experimental details of each of the stopping measurements performed with the three coated detectors, respectively. The energy range and ion species studied are listed, as are the accelerator used, stripping method employed, and the detector bias applied. It should be noted that in the case of the Lund measurements a Wien velocity filter was located between the analyzing magnet and detector set-up.

It is important to note that the results of the measurements indicated by letter 'a' in Table 1 have been reported earlier [7]. However, the peak fitting method has been improved and a new thickness value determined; $(1497 \pm 30) \times 10^{15}$ atoms/cm^2 compared to $(1473 \pm 31) \times 10^{15}$ atoms/cm^2 (an increase of 1.6%). This new value, while not significantly different from the previously determined value, is believed to be a more reliable estimate of the thickness of the Au polkadots. Hence, updated dE/dx values are presented here for these earlier measurements, based on the new thickness estimate and improved fits to the experimental data.

3. Results

(Fig. 2(a)) shows the energy spectrum measured for 7.22 MeV ^{14}N ions incident on the Ge-coated detector.

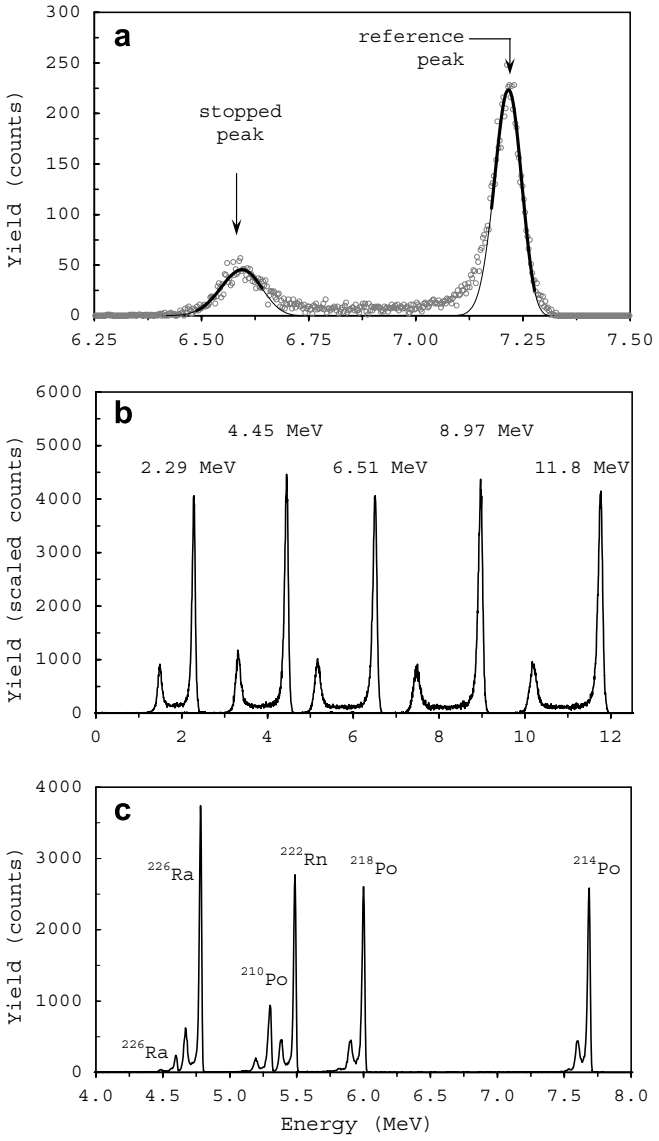

Fig. 2. (a) Energy spectrum showing the stopped and reference peaks for 7.22 MeV ^{14}N ions incident on the Ge-coated detector (unfilled circles). The skewed Gaussian (Gram–Charlier) fits to the two peaks is overlaid (thin solid black line) as well as the regions of interest used in the fit (thick solid black line). (b) Composite energy spectrum for various energy ^{19}F ions incident on the Au-coated detector. (c) Energy spectrum of the alpha particles incident on the Ag-coated detector.

Two peaks are observed. The higher energy peak, hereafter referred to as the 'reference peak', results from ions passing directly into the detector. The lower energy peak, hereafter referred to as the 'stopped peak', is a result of ions that pass through the full thickness of stopping medium before entering the detector. The relative integral areas of these two peaks reflects the areal fraction of the irradiated portion of the detector that is covered in the stopping medium, in this case Ge. The continuous, but low yield, region between these two peaks represents ions that pass through the non-vertical edges of the dots. (Fig. 2(b)) shows a composite spectrum containing the spectra measured for several different energy ^{19}F ions incident on the Au-coated

detector. As the energy of the ion increases so does the energy loss in the Au as evidenced by the increasing spacing between the stopped and reference peaks.

Gram–Charlier series of type A distributions [8] (with zero kurtosis and non-zero skewness) were used to fit the peaks and determine their exact positions. The introduction of a skewness factor was found to more reliably account for the observed scattering tails of the peaks than could be done using a simple Gaussian fit. Only the first few terms of Gram–Charlier series were used. In this form, the truncated series essentially represents a normal probability distribution function multiplied by a factor that incorporates the departure from normality. For the case of zero kurtosis and non-zero skewness the series then has the following form:

$$g = A_0 \cdot \exp\left(-\frac{X^2}{2}\right) \cdot [1 + \alpha(X^3 - 3X)] \quad (1)$$

where

$$X = \frac{x - x_0}{\sigma} \quad (2)$$

The parameters A_0, σ and x_0 have the same meaning as in a Gaussian function, while α is the skewness factor. A negative α value results in a low energy tail, while a positive α results in a high energy tail. In this study it was found that the stopped and reference peaks were approximately equally affected by a (low energy) scattering tail. Hence, the constraint that the skewness factor α has the same (negative) value for the two peaks was applied in each case.

Examples of Gram–Charlier series fits to the stopped and reference peaks are given in (Fig. 2(a)). The extent of the fit lines (thick solid lines) indicates the region of interest that was typically defined in each case in an effort to limit the fits to ions that pass through either a zero or the full thickness of the stopping medium islands and exclude ions that pass though the edges of the islands.

The reference peak positions obtained through these fits were used to calibrate each detector and obtain accurate measurements of the keV/channel values. For the cases where the absolute energy of the ion could not be determined with high precision from accelerator settings (Lund measurements) reference peak positions from the alpha source spectra were used instead. Importantly, no significant departures from linearity were observed and the alpha calibrations for the Lund measurements were found to agree well with the calibration that could be determined from the accelerator settings, indicating that there is no significant pulse height deficit effect for these ions and energies in the PIN diodes and that the alpha calibration is a reliable substitute where a high precision direct calibration is not available.

To determine the final stopping force values from the energy losses measured an accurate estimate of the stopping medium thickness is required. Since alpha particle stopping forces can considered to be well known, the energy loss experienced by the alphas in the stopping medium provides an accurate thickness estimate. This estimate is further improved through the use of a multi-line alpha source (which emits several different energy alpha particles due to the decay of the main isotope and its radioactive daughters) so that 4–6 independent thickness estimates can be combined to provide a best estimate of the thickness. This is illustrated in (Fig. 2(c)) for the Ag-coated detector. Using the alpha particle data thicknesses were determined for the three stopping media. The results are listed in Table 2. Here the uncertainty incorporates the uncertainty in the measurement as well as an estimated 2% uncertainty in the alpha particle stopping powers used.

Table 2
Thicknesses of the three stopping media as measured by alpha energy loss and (for Ge) as measured by proton microprobe measurements

Stopping medium	Thickness: alpha energy loss ($\times 10^{15}$ atoms/cm^2)	Thickness: proton microprobe ($\times 10^{15}$ atoms/cm^2)
Ge	1288 ± 46	1364 ± 71
Ag	1769 ± 36	
Au	1497 ± 30	

From the the proton micropobe backscattering measurements a thickness for the Ge detector of $(1364 \pm 71) \times 10^{15}$ atoms/cm^2 was obtained. The results rely on comparison with a Pt standard (MicroMatter, accurate to $\pm 5\%$) rather than proton stopping force values. Proton microprobe measurements have been performed so far only on the Ge detector but show agreement (within experimental uncertainty) with the thickness measured using the alpha energy loss measurements (see Table 2). (Fig. 3(a)) presents the map of the backscattered protons corresponding to scattering from Ge. From the uniform grey contrast in the central region of the dot (Fig. 3(a)) and the extent of the scatter of data points about the line relative to the counting statistical error (error bars in (Fig. 3(b)) and (c)) there is no evidence to suggest the Ge film thickness not uniform over the central part of the polka-dot. The edges of the Ge dot are sloping which may be associated with edge broadening from the proximity mask used for evaporation. We expect similar thickness profiles for the Au and Ag coated detectors because these were evaporated using identical conditions as used for the Ge coated detector.

Stopping force values have been calculated by dividing the energy loss values by the best estimate of the thickness of the stopping medium on each detector, respectively. This assumes that the change in stopping force is approximately linear over the thickness of the stopping medium, which is a good assumption. The results are plotted in (Figs. 4–6) for the targets Ge, Ag and Au, respectively, and are tabulated at the end of this paper (Table 3).[1] Note that the data

[1] The stopping force results are given in absolute units of eV/(10^{15} atoms/cm^2). Using the target density these can be converted to units incorporating physical thickness such as eV/nm. For example, if the density of your Au target is 5.904×10^{22} atoms/cm^3, multiply the Au stopping force by 5.904 to convert it to units of eV/nm.

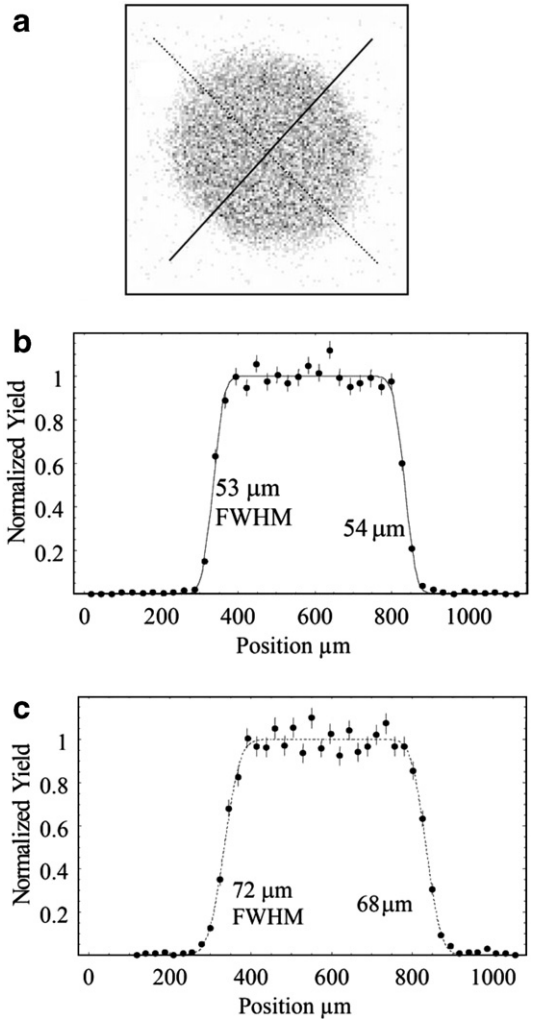

Fig. 3. (a) Map of the backscattered 2 MeV proton signal corresponding to Ge. (b) and (c) line scans of the Ge signal corresponding to the lines shown in (a).

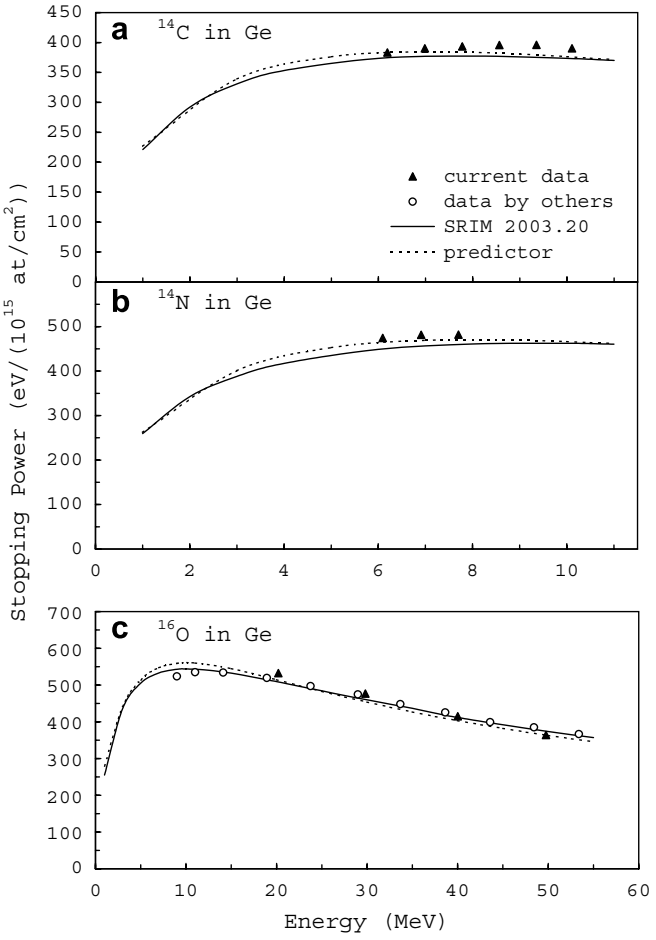

Fig. 4. Stopping force in eV/(10^{15} atoms/cm^2) versus ion energy in MeV for (a) ^{14}C, (b) ^{14}N and (c) ^{16}O ions stopped in Ge. Current data shown as filled triangles, measurements by others as unfilled circles, SRIM 2003.20 predictions as solid lines and predictions by the Weijers et al. predictor [10] shown as dashed lines.

for 49.5 MeV ^{16}O ions stopped in Au were inadvertently taken at a different gain setting to the remainder of the data. The result is included here with our best estimate of the gain change based on the shift in the alpha particle spectra.

In (Figs. 4–6) the stopping forces are plotted at the mean ion energy (incident ion energy minus half the energy loss in the layer). Also plotted in these figures are the stopping forces from the works of others. Data points are taken from the Paul stopping database [11] and stopping force predictions from SRIM2003.20 [6] and the Weijers et al. predictor [10]. Note that in some cases the predictor is plotted outside its optimized validity range (0.1–1.0 MeV/u), however, it is interesting to make this comparison nonetheless.

4. Discussion

For the stopping forces of Ge for ^{14}C and ^{14}N ions shown in (Fig. 4(a) and (b)) there are no other experimental data available from the database suggesting that these measurements are first for these ions in Ge. In general the stopping forces measured tend to be slightly higher than the values predicted by SRIM. The deviation is of the order of 2.3–5.3% for ^{14}C and 4.7–5.3% for ^{14}N. The Weijers et al. predictor does a better job in comparison to the new measurements particularly for ^{14}N, however, the agreement is still not exact.

For the Ge stopping force measurements shown in (Fig. 4(c)) for ^{16}O ions there is one set of experimental data available from the database. The new data spans a comparable energy range on the high energy side of the stopping peak, however, it exhibits a steeper energy dependence than predicted by SRIM or the other data set. Interestingly, the Weijers et al. predictor, which is based on global fit to all of the data in the Paul database, also predicts a steeper energy dependence.

The stopping forces of Ag for ^{14}N and ^{19}F (Fig. 5(a) and (b)) have been studied more thoroughly, though most of the experimental data is concentrated in the energy region below the region of interest here. Around the Bragg peak,

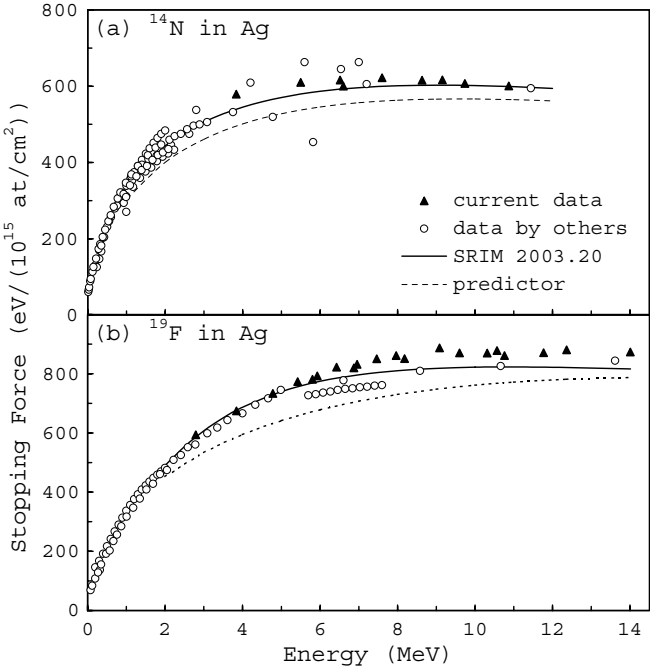

Fig. 5. Stopping force in eV/(10^{15} atoms/cm^2) versus ion energy in MeV for (a) ^{14}N and (b) ^{19}F ions stopped in Ag. Current data shown as filled triangles, measurements by others as unfilled circles, SRIM 2003.20 predictions as solid lines and predictions by the Weijers et al. predictor [10] shown as dashed lines.

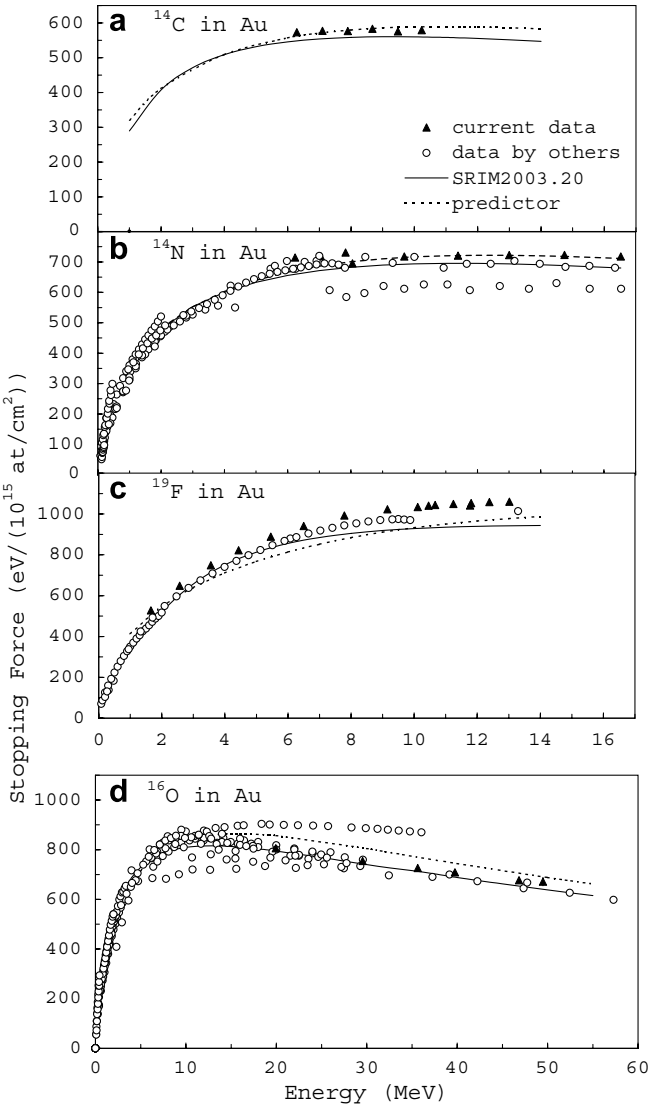

Fig. 6. Stopping force in eV/(10^{15} atoms/cm^2) versus ion energy in MeV for (a) ^{14}C, (b) ^{14}N, (c) ^{19}F and (d) ^{16}O ions stopped in Au. Current data shown as filled triangles, measurements by others as unfilled circles, SRIM 2003.20 predictions [6] as solid lines and predictions by the Weijers et al. predictor [10] shown as dashed lines.

where the current measurements have been performed, comparative data is sparse and shows significant spread. This is particularly true for ^{14}N. The new data is much smoother and generally follows the trend predicted by SRIM, with a significant deviation (up to 6.9%) only at the lowest energies measured. For ^{19}F the new measurements smoothly extrapolate from the energy dependence observed for the other data in the energy range up to 5 MeV. Above 5 MeV the deviation from SRIM becomes significant (increasing upto 7.8% at its maximum). The Weijers et al. predictor does not do as well for this stopping medium for ^{14}N and ^{19}F ions.

For the stopping forces of Au for ^{14}C ion plotted in (Fig. 6(a)) the data is higher than SRIM and in approximate agreement with the Weijers et al. predictor except for the two highest energies where it falls approximately midway between the two. In this case also, the database provides no comparative experimental data suggesting that this is a first measurement for this ion-target combination.

Above 7.5 MeV, existing measurements from the database for the stopping force of Au for ^{14}N ions are in disagreement. Two series of measurements exist, which differ by 10–15%. SRIM and the Weijers et al. predictor suggest that the higher of the two is the most accurate and these are also consistent with data below this energy range. The Au stopping forces measured here (Fig. 6(b)) for ^{14}N ions confirm that the higher of the two sets is the most accurate. The measured data agrees well with the Weijers et al. predictor and suggests that SRIM underestimates the stopping forces of Au by 1.8–6.4% for ^{14}N ions over this energy range.

The stopping measurements for ^{19}F ions in Au plotted in (Fig. 6(c)) show the greatest deviation from SRIM values observed in this study (upto 11.2%). Most of the earlier experimental data for this ion-target combination is concentrated in the energy region below 2 MeV. Recent measurements (2005) by Zhang et al. [12] also indicate that above 2 MeV the SRIM values lie too low, but Zhang et al. suggest a smaller deviation. Our work provides new results in the energy range 10–13 MeV. Our new data, the Weijers et al. predictor and the data by Zhang et al., although not in quantitative agreement, all predict a steeper energy dependence than is expected from SRIM for ^{19}F ions in Au.

Table 3
List of the measured stopping force values (in the units eV/(10^{15} atoms/cm^2)) for various ions and energies in Ge, Ag, and Au, compared with the predictions of SRIM 2003.20 [6] and the Weijers et al. predictor [10]

Stopping medium	Ion species	Mean energy (MeV)	Stopping force in eV/(10^{15} at/cm^2)		
			Measured	SRIM 2003.20	Weijers predictor
Ge	^{14}C	6.19	383.46	374.33	383.26
		6.99	390.23	376.75	381.03
		7.78	393.53	377.19	384.15
		8.56	395.93	376.53	382.35
		9.35	396.19	375.09	379.54
		10.10	390.21	373.15	376.22
Ge	^{14}N	6.09	474.64	449.61	464.45
		6.91	481.42	455.90	468.93
		7.70	481.93	459.51	470.66
Ge	^{16}O	20.20	532.62	508.30	513.28
		29.80	477.10	460.63	454.69
		40.02	414.93	411.83	403.04
		49.76	363.99	374.48	363.75
Ag	^{14}N	3.83	579.38	539.54	495.09
		5.50	609.99	579.51	537.67
		6.51	616.02	592.21	552.04
		6.60	600.46	592.90	553.02
		7.60	622.28	599.15	561.19
		8.63	615.80	602.03	565.44
		9.16	616.84	602.37	566.36
		9.74	607.35	601.82	566.56
		10.89	600.55	598.93	564.97
Ag	^{19}F	2.79	593.62	585.64	518.61
		3.84	674.45	675.85	585.74
		4.78	733.44	729.26	632.02
		5.42	773.10	755.82	657.91
		5.80	781.16	768.14	671.49
		5.93	792.63	772.08	675.86
		6.43	821.98	784.89	691.45
		6.87	819.95	793.94	703.71
		6.95	831.81	795.51	705.80
		7.46	850.50	802.76	718.22
		7.96	861.38	809.63	728.98
		8.18	850.85	811.57	733.31
		9.08	887.42	818.38	748.70
		9.60	870.69	820.48	756.08
		10.32	870.08	822.35	764.70
		10.57	878.47	822.62	767.30
		10.76	861.11	822.79	769.15
		11.77	871.30	822.25	777.32
		12.36	880.69	821.18	780.95
		14.01	873.17	816.11	787.35
Au	^{14}C	6.29	573.06	548.42	561.35
		7.10	577.37	554.58	571.67
		7.90	576.90	558.17	579.01
		8.68	583.34	559.88	587.14
		9.48	575.50	560.30	583.93
		10.23	579.19	559.74	588.75
Au	^{14}N	6.23	714.66	659.61	672.70
		7.05	718.32	672.03	688.31
		7.83	730.82	680.48	699.70
		8.05	695.37	682.65	702.39
		9.69	717.99	692.22	716.57
		11.39	720.98	695.15	722.89
		13.00	722.55	693.53	723.46
		14.75	722.73	688.12	719.99
		16.53	717.69	680.13	713.45

Table 3 (*continued*)

Stopping medium	Ion species	Mean energy (MeV)	Stopping force in eV/(10^{15} at/cm^2)		
			Measured	SRIM 2003.20	Weijers predictor
Au	^{16}O	19.94	806.16	794.56	856.60
		29.54	754.74	742.74	807.14
		35.64	726.27	712.22	770.07
		39.75	709.13	689.65	745.41
		46.84	676.96	653.47	704.99
		49.49	671.36	640.64	690.73
Au	^{19}F	1.66	527.54	461.62	507.83
		2.57	648.68	603.68	603.00
		3.56	749.17	713.44	681.43
		4.43	821.96	779.91	736.56
		5.45	888.73	834.04	789.47
		6.50	941.27	871.57	833.89
		7.79	992.97	900.64	877.73
		9.15	1023.29	920.33	913.93
		10.12	1034.14	929.30	934.71
		10.46	1040.43	931.52	941.15
		10.66	1043.63	932.88	944.74
		11.25	1049.24	936.17	954.58
		11.77	1041.62	938.37	962.35
		11.80	1053.69	938.47	962.78
		12.38	1058.31	940.37	970.50
		13.02	1060.23	941.98	978.01

For our last ion-target combination, ^{16}O stopped in Au (Fig. 6(d)), the comparative data from the database is also concentrated at energies lower than those studied here. Significant spread is also evident particularly around the Bragg peak. The new measurements agree well with both SRIM and those experimental results in the energy range of interest, with a slight deviation (3.2–5.0%) only at the highest energies studied. Clearly, the Weijers et al. predictor does not perform as well. Since the predictor is based on a fit to all reliable data, it tends to be higher in this case as it has been influenced by the anomalously high data set observed just above the Bragg peak.

In general, while there is some scatter in the measured data, the main source of uncertainty is the stopping medium thickness estimate. For the Ge-coated detector, the proton microprobe measurements agree within uncertainty with alpha energy loss measurements, however, some uncertainty in the final stopping force values remains. One advantage of the current technique is that since all the measurements for a given target material are measured on the same target, the measurements form a self-consistent set. This has the added advantage that any future improvements in the thickness measurement can be incorporated subsequently to improve the global uncertainty in the data set.

In this context, it should be noted that the PIN detectors used in this study have proved to be radiation hard, with no measurable degradation in the performance observed thus far. One single detector can therefore be used for large series of measurements providing a set of self-consistent set of results directly comparing the stopping forces for the same stopping medium.

5. Conclusion

In this work a recently-developed novel technique employing coated PIN diodes has been employed to make measurements of the stopping forces in different targets for low energy heavy ions. The technique has proved reliable and efficient for this purpose and a set of self-consistent measurements were obtained for ^{14}C, ^{14}N and ^{16}O ions stopped in Ge, ^{14}N and ^{19}F ions stopped in Ag and ^{14}C, ^{14}N, ^{16}O and ^{19}F ions stopped in Au. Small but significant deviations from SRIM values were observed. Comparisons were also made with a recently-developed empirical stopping force predictor. The predictor performs well even outside its optimized validity range (0.1–1.0 MeV/u) and in many cases agrees more closely with the measured stopping force values than SRIM in the energy range of interest.

Acknowledgement

T.W.-D. and D.J.O. would like to acknowledge the financial support provided by an Australian Research Council Discovery Grant. Travel support from the Royal Physiographical Society in Lund for H.J.W., H.T. and T.W.-D. is gratefully acknowledged. This work was supported by the Academy of Finland under the Finnish Centre of Excellence Programme 2000–2005 (Project No. 44875, Nuclear and Condensed Matter Physics Programme at JYFL).

References

[1] P. Sigmund, Stopping of Heavy Ions a Theoretical Approach, Springer, Berlin, 2004.

[2] F. Hubert, R. Bimbot, H. Gauvin, Atom. Data Nucl. Data Tables 46 (1990) 1.
[3] L.C. Northcliffe, R.F. Schilling, Nucl. Data Tables A 7 (1970) 233.
[4] H. Paul, MSTAR – Stopping power for light ions. Available from: <http://www.exphys.uni-linz.ac.at/stopping/>.
[5] J.F. Ziegler, J.P. Biersack, U. Littmark, The Stopping and Range of Ions in Solids, Vol. 1, Pergamon Press, New York, 1985.
[6] J.F. Ziegler, SRIM version 2003.10, 2003. Available from: <http://www.srim.org>.
[7] H. Timmers, K. Stenström, M. Graczyk, H.J. Whitlow, Nucl Instr. and Meth. B 219&220 (2003) 263.
[8] M.G. Kendall, The Advanced Theory of Statistics, Vol. 1, Griffin, London, 1948, p. 146.
[9] T.D.M. Weijers, T.R. Ophel, H. Timmers, R.G. Elliman, Nucl. Instr. and Meth. A 483 (2002) 676.
[10] T.D.M. Weijers, B.C. Duck, D.J. O'Connor, Nucl. Instr. and Meth. B 215 (2004) 35.
[11] H. Paul, Database of Stopping Power Measurements. Available from: <http://www.exphys.uni-linz.ac.at/stopping/>.
[12] Y. Zhang, W.J. Weber, A. Razpet, G. Possnert, Nucl. Instr. and Meth. B 227 (2005) 479.